ACS APPLIED MATERIALS & INTERFACES

Research Article

www.acsami.org

Influence of the Surface Functional Group Density on the Carbon-Nanotube-Induced α-Chymotrypsin Structure and Activity Alterations

Xingchen Zhao,[†] Fang Hao,[†] Dawei Lu,[†] Wei Liu,[‡] Qunfang Zhou,*[,†] and Guibin Jiang[†]

[†]State Key Laboratory of Environmental Chemistry and Ecotoxicology, Research Center for Eco-Environmental Sciences, Chinese Academy of Sciences, Beijing 100085, P. R. China

[‡]Institute of Chemical Safety, Chinese Academy of Inspection and Quarantine, Beijing 100124, P. R. China

Supporting Information

ABSTRACT: Because of the special properties of carbon nanotubes (CNTs), their applications have been introduced to many fields. The biosafety of these emerging materials is of high concern concomitantly. Because CNTs may initially bind with proteins in biofluids before they exert biological effects, it is of great importance to understand how the target proteins interact with these exogenous nanomaterials. Here we investigated the interaction between α-chymotrypsin (α-ChT) and carboxylized multiwalled CNTs in a simulated biophysical environment utilizing the techniques of fluorescence, UV−vis, circular dichroism spectroscopy, ζ potential, atomic force microscopy, and bicinchoninic acid analysis. It was demonstrated that CNTs interacted with α-ChT through electrostatic forces, causing a decrement in the α-helix and an increment in the β-sheet content of the protein. The protein fluorescence was quenched in a static mode. The increase in the surface modification density of CNTs enhanced the protein absorption and decreased the enzymatic activity correspondingly. α-ChT activity inhibition induced by CNTs with low surface modification density exhibited noncompetitive characteristics; however, a competitive feature was observed when CNTs with high surface modification density interacted with the protein. An increase of the ionic strength in the reaction buffer may help to reduce the interaction between CNTs and α-ChT because the high ionic strength may favor the release of the protein from binding on a CNT surface modified with functional groups. Accordingly, the functionalization density on the CNT surface plays an important role in the regulation of their biological effects and is worthy of concern when new modified CNTs are developed.

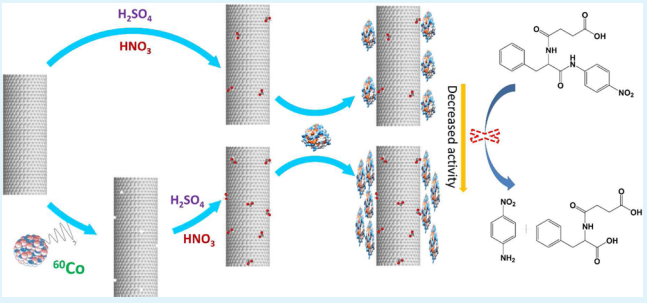

KEYWORDS: *α-chymotrypsin, carbon nanotubes, functionalization density, protein structure, enzymatic activity*

INTRODUCTION

Carbon nanotubes (CNTs) exhibit unique surface, mechanical, optical, chemical, thermal, and electrical properties. As a kind of attractive nanomaterial, CNTs have multiple applications in a wide variety of disciplines such as physics, biology, chemistry, engineering, and medicine. In spite of these excellent features, the toxicity of CNTs is a primary concern because of their possible exposure to human beings through diverse routes. CNTs are reported to elicit toxicity through inducing (1) membrane and DNA damage, (2) reactive oxygen species generation and oxidative stress, and (3) alterations of the mitochondrial activities, intracellular metabolic routes, and protein synthesis.[1−8] Discrepancies in the CNT toxicity studies, both in vivo and in vitro, have been attributed to various factors including the nanomaterial size, surface chemistry, concentration, exposure duration, stimulation method, aggregation degree, and impurities. The functionalization density may also play an important role in the biological responses after CNTs enter biofluids and organisms.

In medical areas, pristine CNTs have limited application because of their poor solubility and biocompatibility. The chemical and biological functionalization of CNTs help to solve these problems to a great extent, thus decreasing the adverse effects.[9,10] However, little is known about how functionalization influences the structure and function of the related enzymes in organisms. A new class of bioactive CNTs conjugated with proteins have recently been generated,[11,12] which shows the possibility of the potential binding of CNTs with these biomacromolecules. Nanobiological device recognition and the binding of nanomaterials with biologically important proteins constitute the first step in the complex mechanism for their pharmacological or toxicological effects.[13,14] Therefore, it is of great value to investigate the interactions between CNTs and biologically valuable proteins.

Received: July 1, 2015
Accepted: August 7, 2015
Published: August 7, 2015

DOI: 10.1021/acsami.5b05895
ACS Appl. Mater. Interfaces 2015, 7, 18880−18890

α-Chymotrypsin (α-ChT) is an important digestive enzyme component in pancreatic juice, and it performs proteolysis in the duodenum. It is commonly used as an excellent enzyme model for studying the nanomaterial-induced enzymatic activity inhibition because of its well-defined structure and extensively characterized enzymatic properties. In this work, we focused on the structure and activity changes of α-ChT when they were absorbed onto multiwalled carbon nanotubes (MWCNTs) with gradient functionalization densities. A combination of techniques like fluorescence, circular dichroism (CD) spectroscopy, ζ-potential analysis, atomic force microscopy (AFM), and bicinchoninic acid (BCA) assay was used to detail the interaction between CNTs and α-ChT in the hope of revealing the role of the CNT functional group density. The findings regarding the protein structural and activity alterations provide fundamental understandings for the toxicological effects of CNTs.

EXPERIMENTAL SECTION

Reagents. MWCNTs (purity more than 95%; diameter 10−20 nm) were bought from Shenzhen Nanotech Port Co., Ltd. (Shenzhen, China). α-Chymotrypsin (α-ChT) from bovine pancreas, phosphate-buffered saline (0.138 M NaCl, 0.0027 M KCl; pH 7.4 at 25 °C), *N*-succinyl-L-phenylalanine *p*-nitroanilide, and *p*-nitroaniline were all purchased from Sigma-Aldrich (St. Louis, MO). A Micro BCA Protein Assay Kit from Thermo Scientific (Rockford, IL) was used to determine the supernatant protein concentration after centrifugation at 8000 rpm for 20 min. Other chemical reagents were obtained from Sinopharm (Beijing, China). Ultrapure water (resistance of more than 18.2 MΩ cm^{-1}) was used throughout the experiments.

Purification and Modification of CNTs. A pristine CNT (1 g) was purified with 200 mL of nitric acid (about 65%) at 60 °C for 10 h. Purified CNTs were washed with ultrapure water and then irradiated with ^{60}Co. Irradiation was performed on a ^{60}Co irradiator (31.5 GBq in total activity at the irradiation center; Shandong Academy of Agricultural Sciences) for 48 h. The distance between the CNT samples and ^{60}Co irradiator was adjusted to obtain different irradiation doses ranging from 50 to 250 kGy. γ-rays from the ^{60}Co irradiator were used to generate defects on the CNT surfaces by breaking C−C bonds.[15] γ photons possess high kinetic energy and can produce the Compton effect as well as the photoelectric effect with the creation of electron−hole pairs. Chemical modification was then conducted on the CNTs with different defects. A total of 0.9 g of the purified MWCNTs was subjected to 500 mL of a H_2SO_4/HNO_3 (3:1) mixture and sonicated at 60 °C for 25 h. In this process, the H_2SO_4/HNO_3 mixture, as the oxidizing agent, reacted with the defected graphite surface and created carboxyl groups, thus forming covalent modification on CNTs. The resultant suspension was poured into 400 mL of water afterward, and the larger-cut MWCNTs were collected on a 220-nm-pore filter membrane and rinsed with a 20 mM NaOH solution. Finally, the soluble powder was obtained by vacuum drying. The concentrations of CNTs in the stock solution were determined by measuring the optical densities of the dispersion at 907 nm, as illustrated in our previous study.[16]

Transmission Electron Microscopy (TEM) Characterization. The morphology of MWCNTs was photographed using a JEM-2100 transmission electron microscope (JEM, Japan) with an accelerating voltage of 200 kV. Samples dispersed on the copper nets, which were precoated with carbon film, were dried overnight in vacuum before TEM observation.

Fourier Transform Infrared (FTIR) Spectroscopy Analysis. CNT powder was mixed with KBr in an agate mortar and then pressed to form a pellet. The FTIR spectra were recorded on a FTIR-8400S spectrometer (Shimadzu, Japan). All spectra were taken via the ATR method in the range of 400−2800 cm^{-1} with a resolution of 1 cm^{-1}.

ζ-Potential Measurement. ζ-potential analysis of MWCNTs was performed using the Malvern Nanosizer ZS instrument (Malvern, U.K.). A protein solution was freshly prepared and titrated with 0.02 M Tris-HCl buffer to adjust the pH values from 4.5 to 8.5. CNTs were then added, and the whole solution was calibrated to 10 mL with distilled water for final analysis. The ζ potential was calculated automatically by the instrument based on the following Henry equation:[17]

$$\mu_E = \frac{2\varepsilon\zeta f(\kappa\alpha)}{3\eta}$$

where μ_E is the electrophoretic mobility, ε is the dielectric constant, ζ is the zeta potential, and η is the viscosity of the solution. The function $f(\kappa\alpha)$ stands for Henry's corrective term.

AFM Analysis. AFM images were taken using an Agilent 5420 AFM instrument (Santa Clara, CA) with probes at a scan frequency of 342 kHz. The instrument was operated in the tapping mode using the pyramidal cantilever with a silicon probe at the tip. Samples were prepared by adding 20 μL of the mixture onto mica plates and drying under an IR lamp.

Free Protein Concentration Analysis. CNT (10 mg L^{-1}) was mixed with a 2 μM protein solution and was shaken for 1 h at 25 °C. After incubation, the mixture was subjected to centrifugation at 7000 rpm for 15 min. The supernatant was obtained for free protein concentration determination using a Pierce BCA Protein Assay Kit from Thermo Scientific (Waltham, MA).

Spectroscopic Measurements. Fluorescence spectra were measured on a Hitachi F-4600 fluorescence spectrophotometer (Hitachi, Japan). Signals were recorded with the excitation and emission slits at 5.0 nm. The protein−CNT mixture was excited at 280 nm to obtain information on the Tyr, Phe, and Trp residues. The scanning speed was fixed at 1200 nm s^{-1} within the range of 290−420 nm.

Inner filter effects (IFEs), which cause both excitation and emission absorbance in fluorescence measurements, were taken into consideration here:[18]

$$F_{ideal}(\lambda_{ex}, \lambda_{em}) = F_{obs}(\lambda_{ex}, \lambda_{em})\, CF_p(\lambda_{ex})\, CF_s(\lambda_{em}) \approx F_{obs}(\lambda_{ex}, \lambda_{em}) \times 10^{(A_{em}+A_{ex})/2}$$

where F_{ideal} is the fluorescence density after elimination of IFEs, F_{obs} is the fluorescence density detected directly by the instrument, CF_p is the correction factor for the absorbance of the sample at the excitation wavelength λ_{ex}, and CF_s is the correction factor for the absorbance of the sample at the emission wavelength λ_{em}. A_{ex} and A_{em} stand for absorbance values at the fluorescence excitation and emission wavelengths, respectively.

The data were further investigated using the Stern−Volmer equation:[19,20]

$$\frac{F_0}{F} = 1 + K_{SV}[Q] = 1 + k_q\tau_0[Q]$$

where F_0 and F are the fluorescence intensities in the absence and presence of quencher, respectively, K_{SV} and k_q are the Stern−Volmer quenching constant and the quenching rate constant, respectively, [Q] is the quencher concentration, and τ_0 is the lifetime of the fluorophore in the absence of quencher.

The UV−vis spectra were measured using a Shimadzu UV 2450 spectrophotometer (Shimadzu, Japan) and corrected by the background. All of the protein data were collected from 350 to 190 nm with a scanning speed of 400 nm min^{-1} and a slit of 0.2 nm.

CD measurements were performed on a J-810 spectropolarimeter (Jasco, Japan) under a constant nitrogen flush. The spectra were recorded using a 1-cm-pathway quartz cell from 260 to 200 nm with a 1 nm interval at 298 K. The final spectrum of each system was the average of two runs. Raw data obtained in millidegrees were converted to mean residue ellipticity (MRE) using the formula:[21]

$$MRE = \frac{\theta_{obs}}{10ncl}$$

where θ_{obs} is the raw data obtained from the instrument in millidegrees, n is the amino acid residue number, c is the protein

DOI: 10.1021/acsami.5b05895
ACS Appl. Mater. Interfaces 2015, 7, 18880−18890

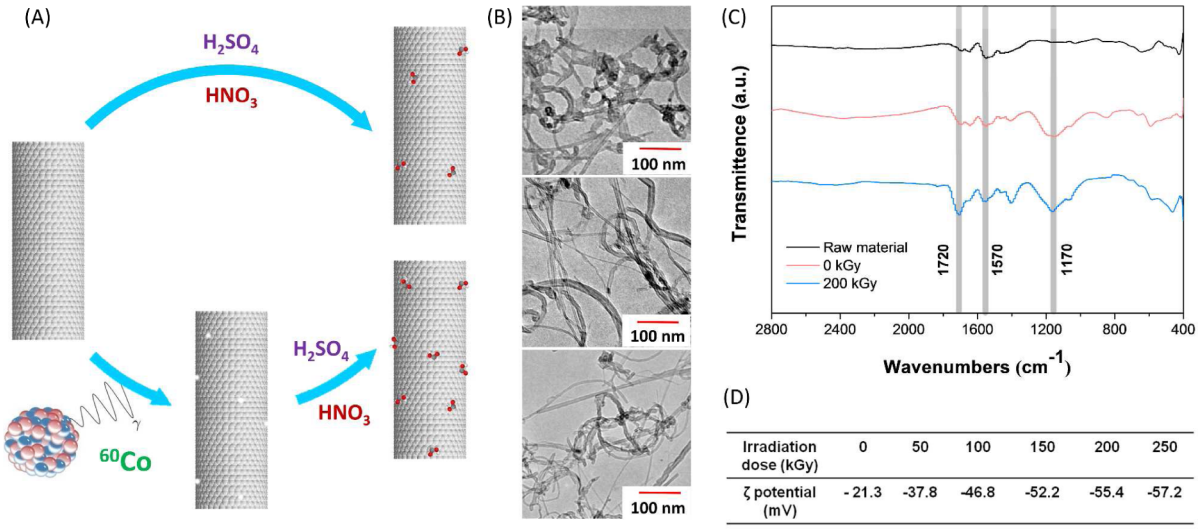

Irradiation dose (kGy)	0	50	100	150	200	250
ζ potential (mV)	-21.3	-37.8	-46.8	-52.2	-55.4	-57.2

Figure 1. (A) Scheme of CNT modification. (B) TEM characterization of CNTs before (upper) and after carboxylation (middle, 0 kGy; bottom, 200 kGy). (C) FTIR spectra and (D) ζ potentials of naked and modified CNTs (pH 7.4).

concentration, and *l* is the light pathway in centimeters. The data were analyzed using the *CDpro* software package.

Enzymatic Activity Assay. Using *N*-succinyl-L-phenylalanine *p*-nitroanilide as the substrate, the enzymatic activities of α-ChT with and without CNT treatments were evaluated by measuring the product generation of *p*-nitroaniline at a maximum absorbance of 405 nm. On the basis of this spectral character, the enzymatic activity was evaluated by monitoring the absorbance during 2 min after the addition of protein to the substrate. Kinetic constants were calculated by fitting the initial rates to the Michaelis−Menten equation. The initial reaction velocity (v_0) was obtained from the linear part of the equation:[22]

$$v_0 = \frac{V_{max}[S]}{K_m + [S]}$$

where V_{max} is the maximum velocity of the reaction, [S] is the substrate concentration, and K_m is the Michaelis−Menten constant, which equals the substrate concentration when the reaction rate is half of V_{max}. The Lineweaver−Burk double reciprocal plot is drawn to judge the enzymatic inhabitation mode:[23]

$$\frac{1}{v_0} = \frac{K_m}{V_{max}[S]} + \frac{1}{V_{max}}$$

RESULTS AND DISCUSSION

Characterization of Modified CNTs. Figure 1A illustrates the modification process of the CNTs. The modified CNTs were prepared by the incubation of a H_2SO_4/HNO_3 mixture with pristine CNTs with or without ^{60}Co irradiation. CNTs with different modification densities were characterized by TEM, FTIR, and ζ-potential analysis. Figure 1B shows the TEM images of raw CNTs (upper panel) and modified CNTs with 0 kGy (middle panel) and 200 kGy (bottom panel) irradiation. Raw CNTs were attached with amorphous carbon and other impurities (Figure 1B, upper panel). However, after purification and chemical modification on the surface, the CNTs became neater, tidier, and shorter (Figure 1B, middle and bottom panels). The surface morphology was not obviously altered by high doses of irradiation (Supporting Information, Figure S1); nevertheless, more carboxyl groups were substantially modified onto the CNT surfaces, as evidenced from Figure 1C. The peak at 1570 cm^{-1} is attributed to the C═C stretching of CNT sidewall defects. The peak at 1720 cm^{-1} clearly shows the C═O stretching mode for the modified CNTs, and the strong absorption peak at about 1170 cm^{-1} is associated with the stretching of C−O, indicating the successful modification of the carboxyl groups on the graphene walls and to the edges of the holes.[16] It is commonly believed that the higher the irradiation dose is, the more chemical modification is produced.[24] This was evidenced by the finding that the stretching signals of C═O and C−O increased with the irradiation dose in this work. This phenomenon was also confirmed by ζ-potential measurements (Figure 1D), wherein the ζ potential of the modified CNTs decreased with an increase of the irradiation dose, showing that more C═O groups were modified onto the surface of CNTs.

Protein−CNTs Bioconjugate Analysis. In order to understand the morphology of the protein−CNTs complex and figure out whether the adsorption behavior of α-ChT onto CNTs is functionalization-density-dependent, we conducted AFM analysis. The height profile of the protein molecules on the CNTs was displayed in Figure 2. AFM gives a topographical image, showing the height of naked CNTs varied from 10 to 20 nm (indicated by a blue line), which is in line with TEM observations. The height of the CNTs layer on the surface varied significantly with the carboxyl density (marked by a green line). The three-dimensional sizes of α-ChT are 5.1 × 4.0 × 4.0 nm; however, height analysis demonstrated that the layer height was 3.1 nm (probably monolayer) in the 0 kGy group (Figure 2B), which was different from any dimension of the protein. It was thus assumed that the protein molecules got unfolded and packed onto CNTs, forming protein coronas around the CNT surfaces.[25] As the functionalization density increases, the protein further forms thicker layers. For example, they were 14.4 and 20.8 nm for 50 and 200 kGy groups (Figure 2D,F), respectively, which were in a positive correlation with the ζ potentials of the CNTs. These results are coincident with the TEM outcomes (Supporting Information, Figure S2). This may indicate a higher propensity of protein aggregation on CNTs with more functional groups.[26] Multiple layers of protein were adsorbed onto 50 kGy (at least three layers) and 200 kGy (at least five layers) radiation-treated CNTs.

However, AFM can only provide qualitative information on part of certain CNTs. In the quest of the coverage density and

DOI: 10.1021/acsami.5b05895
ACS Appl. Mater. Interfaces 2015, 7, 18880−18890

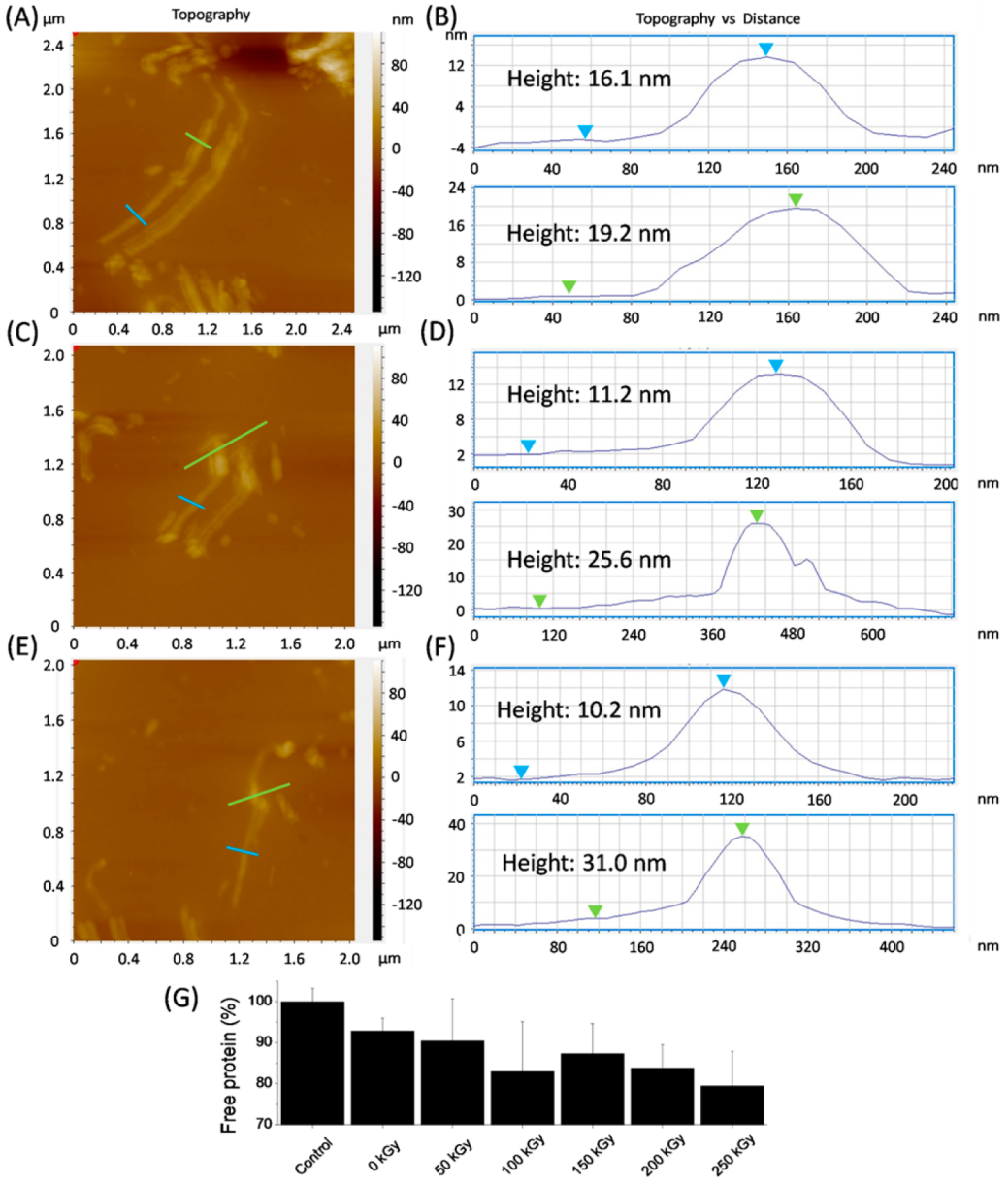

Figure 2. (A–F) Morphology characterization for the complex of CNTs and α-ChT by AFM. (A, C, and E) AFM height images of CNTs treated with 0, 100, and 200 kGy radiation, respectively. The complexes of CNTs and α-ChT protein are marked by green lines, and the pristine CNTs are indicated by blue lines. (B, D, and F) Height comparison of naked CNTs (blue arrows) with a CNTs–protein complex (green arrows). (G) The unbound protein contents in supernatants of an α-ChT and modified CNTs mixture.

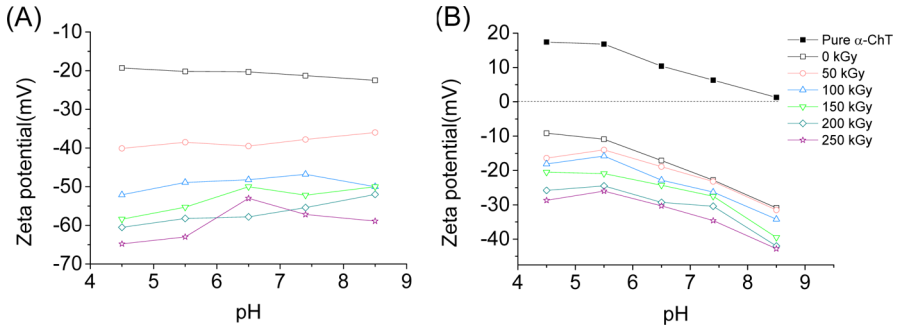

Figure 3. (A) ζ potentials of CNTs with different functional group densities at different pH values. (B) ζ potentials of pure α-ChT and protein–CNTs conjugates at diverse pH values. The final concentrations of α-ChT and CNTs were 2 μM and 10 mg L^{-1}, respectively.

DOI: 10.1021/acsami.5b05895
ACS Appl. Mater. Interfaces 2015, 7, 18880–18890

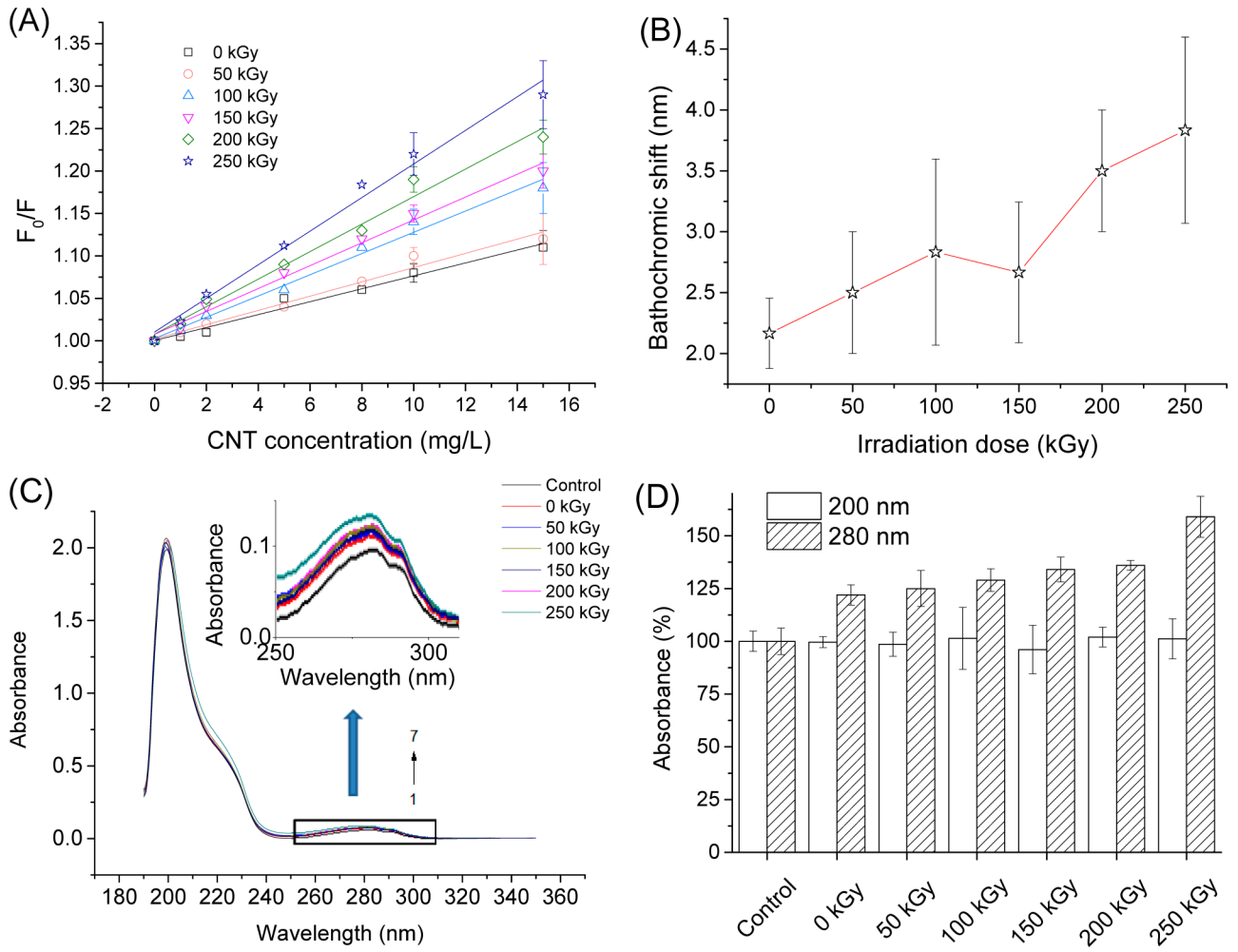

Figure 4. (A) Stern−Volmer plots for α-ChT−CNTs complexes at 340 nm after elimination of IFEs ($C_{\alpha\text{-ChT}}$ = 2 μM; $C_{\alpha\text{-ChT}}$ = 10 mg L^{-1}). (B) Bathochromic shifts of fluorescence spectra of the system. (C) UV−vis absorbance spectra of α-ChT (5.6×10^{-7} M) bound with modified CNTs (2.5 mg L^{-1}). Lines 1−7 show the groups from control to 250 kGy. (D) Calibrated absorbance of α-ChT bound with modified CNTs.

the amount of protein adsorption onto CNTs, we analyzed the free protein concentration in the supernatants of an α-ChT and CNTs mixture using the BCA method. The percentage of protein bound to CNTs was thus calculated. Compared to less modified CNTs, more α-ChT was found to bind onto CNTs with a higher carboxyl density, which was indicated by a decrease in the free protein concentration in the supernatants (Figure 2G). CNT surfaces with the modification of carboxyl groups are negatively charged, while the protein is positively charged at pH 7.4; thus, it is reasonable that CNTs with increased carboxyl density may result in a higher load of protein.[27]

pH-Dependent Binding. The alkalinity of pancreatic juice varies with its secretion rate, providing pH values ranging from ~7 in slowly secreted juice to ~9 in more rapidly secreted juice.[28] When pancreatic juice encounters gastric acid (pH 1−2) in the intestine, it will be neutralized. Thus, it is of great importance to study the biophysical status of α-ChT at different pH values. ζ potentials of modified CNTs with and without α-ChT incubation were evaluated in the pH range of 4.5−8.5. Figure 3A reveals ζ-potential profiles of diverse unconjugated CNTs along the pH values. Because of the nonamphoteric character of CNTs, the protonation of their surface functional groups does not change the charges, and they remain constantly negatively charged in the investigated pH range. Because the Ip (isoelectric point) of α-ChT is about 8.5, it exhibits a positive charge in the tested pH range (Figure 3B). When the conjugates of α-ChT−CNTs were challenged by pH alterations, obvious elevation shifts in the ζ potentials (Figure 3B) were observed in the tested pH range compared to the unconjugated ones (Figure 3A). For example, the pH value was increased by 5−10 mV for α-ChT−CNTs conjugates at pH 8.5 compared to the corresponding naked CNTs, indicating a strong electrostatic interaction between these two substances and the CNT surfaces masked by the protein. The surface charges of α-ChT−CNTs conjugates continuously increased with the increased acidity in the solutions, demonstrating that more protein with positive charges were loaded onto the nanotube surfaces. Accordingly, the electrostatic attraction was considered to be the dominating binding force for the interaction between α-ChT and CNTs. However, it should be noted that some weak interactions like $\pi-\pi$ interaction may also exist. The $\pi-\pi$ interaction can occur between the aromatic rings on the surface of CNTs and the indole structure of chromophore residues, especially for Trp-172 and Trp-215, which is located at the activity site of α-ChT.[29] Besides, other chromophore residues near the protein surface are also likely to be involved.

DOI: 10.1021/acsami.5b05895
ACS Appl. Mater. Interfaces 2015, 7, 18880−18890

Spectrometric Alterations in Protein−CNTs Bioconjugates. It is known that protein fluorescence can be quenched by a wide spectrum of exogenous ligands including nanomaterials.[30−32] The protein aromatic fluorophores such as Phe, Tyr, and Trp are very sensitive to their microenvironment and thus are ideal indicators for study of the protein conformational changes upon binding of the ligands. The quenching of the protein fluorescence density is commonly caused by the ligands through energy transfer or microenvironmental alterations in the protein.[33,34] Incubation of increasing amounts of modified CNTs with α-ChT caused an evident decrease in protein fluorescence (Supporting Information, Figure S3). Figure 4A shows the fluorescence quenching profiles of α-ChT after elimination of IFEs, which was expressed by Stern−Volmer plots. Obviously, the values of F_0/F exhibited linear increases with the concentrations of multiple modified CNTs. The slope of F_0/F increased with the modification density of CNTs, showing that CNT functionalization enhanced the quenching effect on the fluorescence of α-ChT. The Stern−Volmer equation was further used to evaluate the mode of CNT-induced fluorescence quenching of α-ChT. For biomacromolecules, the lifetime is usually calculated as 10^{-8} s. Assuming that the molecular weight of a single CNT is χ, which is larger than 1000, the calculated k_q is much larger than the maximum diffusion collision rate constant 2.0×10^{10} L mol^{-1} s^{-1} (Table 1). Thus, the static quenching mechanism is supposed to be the dominant quenching mode for the CNTs−protein complexes here. This result was confirmed by fluorescence lifetime measurements (Supporting Information, Figure S4), where the lifetime of the protein is constant. Protein−nanomaterial complexation is usually associated with noncovalent interactions, such as hydrogen-bonding, electrostatic, hydrophobic, and π−π-stacking interactions.[27,35−37] Regarding the structures of α-ChT and the CNTs, noncovalent interaction forces were believed to play the dominant roles in the interactions. A similar fluorescence quenching phenomenon was also reported for the interactions of various ligands with proteins.[33,38]

Table 1. Stern−Volmer Quenching Constants of α-ChT−CNTs Interactions at 298 K

	Stern−Volmer quenching constants				
irradiation dose (kGy)	K_q (M^{-1} s^{-1})	K_{SV} (M^{-1})	R^{2a}	RSS[b]	SD[c]
0	$7.60\chi \times 10^8$	7.60χ	0.9854	6.42×10^{-4}	0.0065
50	$8.39\chi \times 10^8$	8.39χ	0.9815	7.35×10^{-4}	0.0103
100	$12.5\chi \times 10^8$	12.5χ	0.9877	3.36×10^{-4}	0.0119
150	$13.5\chi \times 10^8$	13.5χ	0.9848	3.58×10^{-4}	0.0082
200	$16.2\chi \times 10^8$	16.2χ	0.9738	2.82×10^{-4}	0.0121
250	$19.8\chi \times 10^8$	19.8χ	0.9763	2.09×10^{-4}	0.0131

[a]R^2 is the correlation coefficient. [b]RSS is the residual sum of squares. [c]SD is the standard deviation.

The wavelength of the emitted light is a better indication for the environment of the fluorophores. The results in Figure 4B show that a clear bathochromic shift occurred when CNTs were introduced to α-ChT, indicating microenvironmental changes (from a less polar to a more polar environment) around the fluorophore residues. The bathochromic shift tendency was positively correlated with the functionalization of CNTs. This result was consistent with the finding in protein fluorescence quenching (Figure 4A), showing the stronger the interaction between CNTs and α-ChT, the more the protein conformation was perturbed.

UV−vis spectroscopy provides useful information on the protein conformational alterations. As presented in Figure 4C, the strong absorption at 200 nm is associated with a protein polypeptide backbone structure from π → π* electron cloud transition of C═O in peptide bonds, while the weak peak at around 280 nm is related with the n → π* electron cloud transition of the fluorophores.[31,39,40] The inset in Figure 4C shows that the absorbance of the protein at 280 nm increased with the CNT funtionalization density, and the quantitative results are depicted in Figure 4D. This implies that the microenvironmental hydrophilicity of the amino acid residues increased, which is in high agreement with fluorescence findings (Figure 4A). This result is consistent with the findings that the protein absorbance at around 280 nm changed as a result of conjugation formation between the ground-state fluorophore and the quencher during static quenching, while no absorption spectrum change was observed for dynamic quenching.[32] In addition, the backbone peak at 200 nm from the protein samples treated with modified CNTs showed no obvious changes compared to that of native protein (Figure 4D),

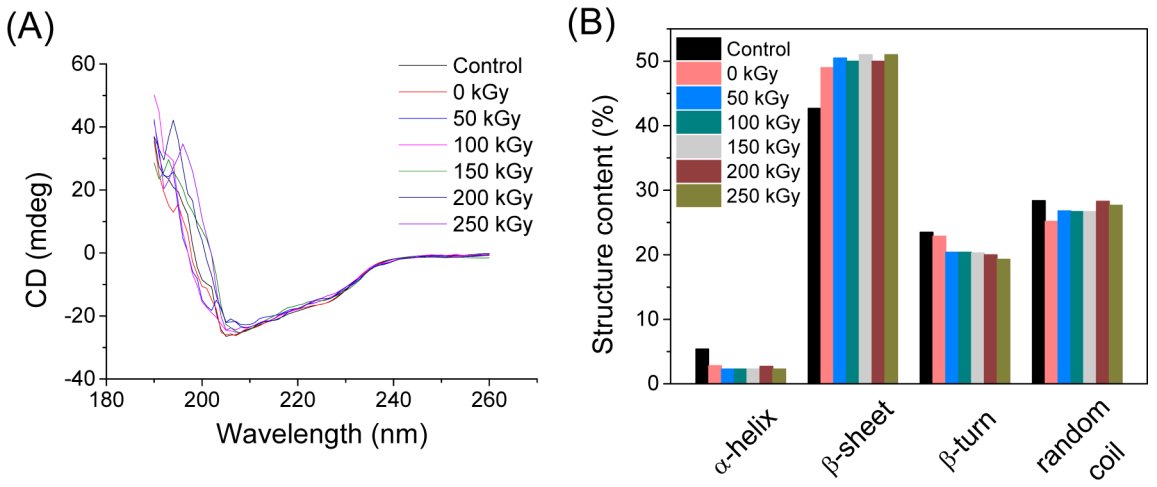

Figure 5. CD spectra of α-ChT (2×10^{-6} M) bound with diverse modified CNTs (10 mg L^{-1}) (A) and ratios for the secondary structure of α-ChT (B).

DOI: 10.1021/acsami.5b05895
ACS Appl. Mater. Interfaces 2015, 7, 18880−18890

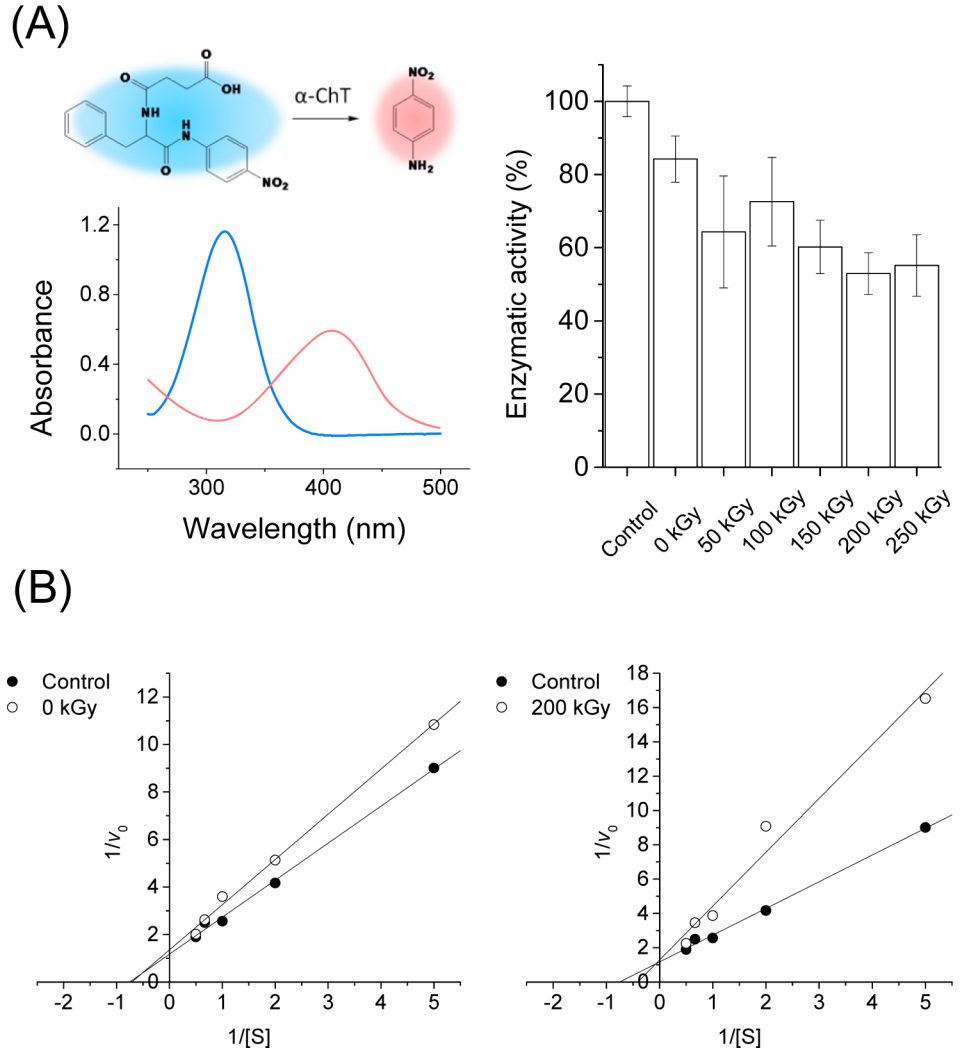

Figure 6. (A) Schematic illustration of the catalytic reaction of α-ChT with the substrate *N*-succinyl-L-phenylalanine *p*-nitroanilide (blue). The enzymatic activity of α-ChT was decreased by the addition of modified CNTs, as was measured by the production of *p*-nitroaniline (red) within 1 min. (B) Lineweaver–Burk plots of α-ChT in the absence (solid circle) and presence (hollow circle) of modified CNTs (0 kGy, left panel; 200 kGy, right panel). The concentrations of α-ChT and CNTs in all of the tests were 2×10^{-6} M and 10 mg L^{-1}, respectively.

suggesting that the amide moieties did not change in the energy gap transition and no resultant skeleton structure alteration occurred.

Conformational Changes of α-ChT Induced by CNTs. CD spectroscopy was applied to investigate the secondary structural changes of α-ChT upon interaction with CNTs. The far-UV CD spectrum of α-ChT was characterized by negative peaks at 229 and 205 nm (Figure 5A). Crystal structure analysis shows that α-ChT is composed of an antiparallel pleated β-sheet, which either is in the form of very short irregular strands or is highly distorted.[41] It is interesting that CNTs cause little alteration in the α-ChT secondary structures including minor α-helical content reduction (~3%) and β-sheet content increment (~7%) (Figure 5B). This phenomenon is usually caused by the destruction of protein hydrogen-bonding networks and the formation of a distorted β-sheet. However, the surface functional group density of CNTs had no effect on the secondary structural alterations of CNTs, as depicted by the similar ratios of α-helix, β-sheet, β-turn, and random coil in α-ChT treated with different CNTs after different doses of irradiation (Figure 5B).

Enzymatic Dynamics of α-ChT Bound onto CNTs. To investigate whether the enzymatic activity of α-ChT is influenced by CNTs and, if it is, which inhibition mode it follows, we carried out enzymatic activity and kinetics studies. Monitoring of the enzymatic activity through the evaluation of *p*-nitroaniline production shows that treatment of CNTs decreased the enzymatic activity of α-ChT by around 18%. The increasing functional group densities were associated with a discernible reduction in the enzymatic activities (Figure 6A). The kinetic constants (K_m and V_{max}) for enzymatic dynamics were obtained by fitting the initial rates and the concentrations of the substrate to the Michaelis–Menten equation, and the reciprocal of the *N*-succinyl-L-phenylalanine *p*-nitroanilide concentration against the reciprocal of the initial reaction rates was plotted as a Lineweaver–Burk plot. The parameters are listed in Table 2. Because V_{max} is unaffected by competitive inhibitors, competitive inhibitors have the same *y* intercept as an uninhibited enzyme, and the intersection of the two lines lies on the *y* axis. Noncompetitive inhibition produces plots with the same *x* intercept as the uninhibited enzyme, where K_m remains the same, and the intersection of the two lines lies on the *x* axis. We chose the data of the 0 and 200 kGy groups for

DOI: 10.1021/acsami.5b05895
ACS Appl. Mater. Interfaces 2015, 7, 18880–18890

Table 2. Lineweaver–Burk Parameters of α-ChT–CNTs Interactions at 298 K

irradiation dose	regression equation	R^2[a]	RSS[b]	SD[c]	K_m	V_{max}
N/A[d]	$1/v_0 = 1.559/([S] + 1.170)$	0.9949	0.1298	0.286	1.332	0.855
0	$1/v_0 = 1.903/([S] + 1.351)$	0.9946	0.2066	0.263	1.409	0.740
50	$1/v_0 = 2.560/([S] + 1.307)$	0.9811	1.3056	0.292	1.959	0.765
100	$1/v_0 = 2.617/([S] + 1.311)$	0.9900	1.4624	0.252	1.996	0.763
150	$1/v_0 = 2.902/([S] + 1.289)$	0.9624	2.3412	0.281	2.251	0.776
200	$1/v_0 = 3.139/([S] + 1.283)$	0.9697	3.1829	0.225	2.447	0.779
250	$1/v_0 = 3.078/([S] + 1.277)$	0.9753	3.5311	0.240	2.410	0.783

[a]R is the correlation coefficient. [b]RSS is the residual sum of squares. [c]SD is the standard deviation. [d]N/A = not applicable.

comparison analysis, and the results are depicted in Figure 6B. For the 0 kGy group, the uninhibited and inhibited enzymes shared similar $1/K_m$ values (0.751 for the control and 0.710 for 0 kGy), which was a feature for uncompetitive inhibition. However, for the 200 kGy group, the inhibition mode is more likely to be a competitive one because the y intercepts were near each other (0.855 for the control and 0.779 for 200 kGy; Figure 6B and Table 2).

Effect of the Ionic Strength on CNT-Induced α-ChT Activity Inhibition. Like pH, the ionic strength is also biologically relevant in biological systems, which varies from 200 to 250 mM in red blood cells, is 150 mM in plasma, and is 3–15 mM in bile.[42] The Results and Discussion section revealed that the interaction between α-ChT and CNTs might be electrostatic forces, and if so, an increase of the ionic strength in the solution would mask the electrostatic forces and block the interaction. To further verify the interaction mode for CNTs and α-ChT, we first incubated the CNTs and protein for 1 h, and then added NaCl to make the final concentration ranging from 0 to 0.5 M. By performing the enzymatic activity tests for these samples, we found that an increase of the salt concentration in the solution gradually restored the enzymatic activity of α-ChT and a platform was reached when the NaCl concentration was elevated above 0.4 M (Figure 7A). The similar increase trend exhibited in the protein activities was inhibited by CNTs with different functional group densities (0–250 kGy). Restoration of the enzymatic activity suggested that the ionic strength could modulate the interaction between the protein and CNTs and the binding was reversible. However, it should be noted that the maximum protein activities in all groups were in the range of 78–86%, indicating that the appended salt did not completely release the protein from CNTs binding and restore their activities at 100%. This phenomenon might be attributed to the fact that preincubation of CNTs and α-ChT caused the partial irreversible denaturation of protein and complete loss in the activities.[43,44]

Comparative experiments upon 1 h of incubation of the ternary system including α-ChT, CNTs, and NaCl, which were mixed at the same time, were performed to avoid the possible initial irreversible binding between the protein and CNTs. The results depicted in Figure 7B showed that, similar to the trend in Figure 7A, an increase of the salt concentration obviously elevated the protein activities. What is more, when the salt concentration was high enough (0.4–0.5 M), the protein activities in all groups were restored as much as 100%, similar to the control (rare CNTs; Supporting Information, Figure S5). The finding suggested that the electrostatic attraction between the protein and CNTs can be attenuated in the presence of competitive ions. The high ionic strength in the solution blocked the protein from binding with CNTs, thus fully preserving its enzymatic activity. Therefore, electrostatic force is the dominant interaction mode for the binding between α-ChT and CNTs, and this interaction was largely reversible upon ionic strength mediation.

Elucidation of the Binding between CNTs and α-ChT. CNTs bound α-ChT at its active pocket through electrostatic and $\pi-\pi$ interactions, and this interaction might alter the structure of the active center and the original spatial arrangement of the amino acid residues (Gly-193, Ser-195, His-57, and Asp-102). The catalytic activities were thus influenced. Inhibition of the enzymatic activity was possibly related with the steric effects of CNTs because the bulk of the CNTs were large enough to block the protein active pocket. Zhang et al. reported that α-ChT specifically bound CNTs through dibutylamino group modification based on the fact that no Trp residue is near the catalytic site of α-ChT according to its crystal structure.[45] However, according to previous

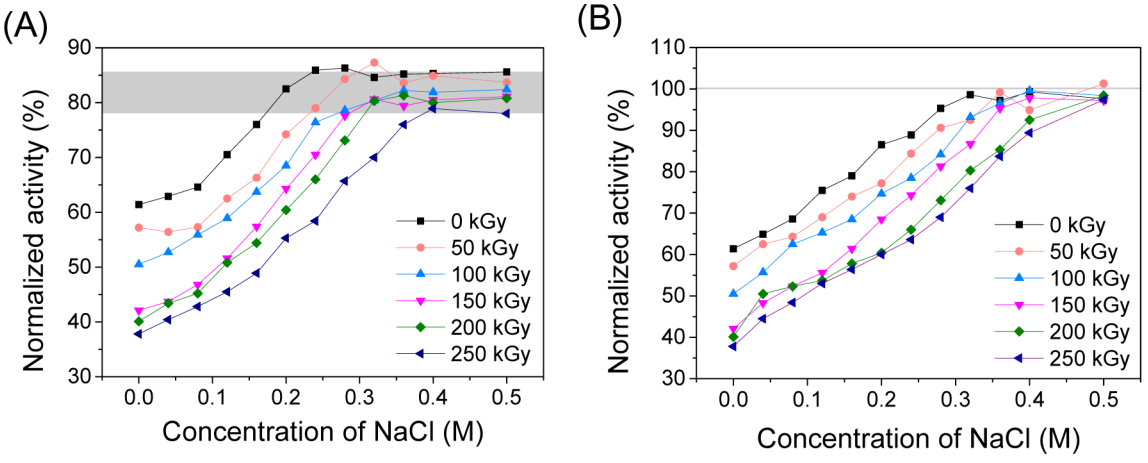

Figure 7. Effects of the ionic strength on the α-ChT activity. α-ChT (2×10^{-6} M) was preincubated (A) and postincubated (B) with CNTs (10 mg L^{-1}) for 1 h in the presence of NaCl.

DOI: 10.1021/acsami.5b05895
ACS Appl. Mater. Interfaces 2015, 7, 18880–18890

research,[29] Trp-172 and Trp-215 are located within 3 Å of the catalytic site of the protein (Figure 8) and form a strong $\pi-\pi$ interaction with the graphene surface; hence, if the catalytic site was perturbed or bound by small molecules, the microenvironment of these Trp residues would be changed, thus causing CNTs binding.

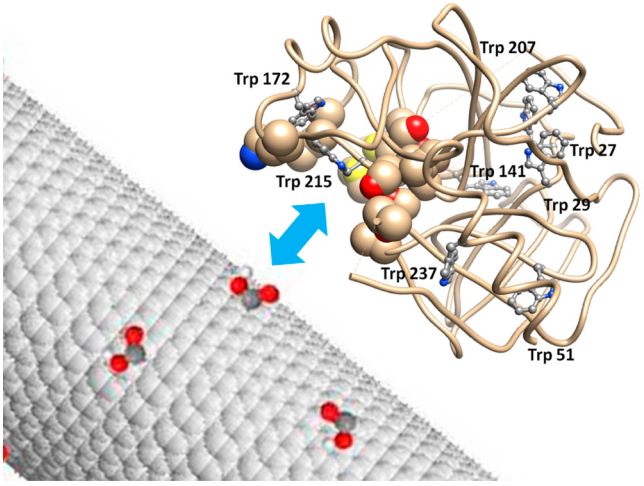

Figure 8. Schematic diagram for the binding of the modified CNTs with α-ChT. The protein structure was obtained from Protein Data Bank ID 4Q2K, the active site was shown in sphere mode, and the Trp residues were shown in ball-and-stick mode by Chimera.

CNTs have strong absorbance in the ultraviolet zone, and the absorption of excitation and/or emission radiation in fluorescence measurement induces IFEs, which may interfere with the fluorescence results of the protein.[16] Zhang et al. discussed the fluorescence results without considering IFEs and took it for granted that CNTs inhibited the enzymatic activity without perturbing the microenvironment of Trp residues. In this study, this problem was avoided by taking IFEs into account during the measurement.

As mentioned above, CNTs with a low density of functionalization inhibit the enzymatic activity in a noncompetitive-like mode, while high-density-functionalized CNTs caused enzymatic activity inhibition in a competitive-like mode. Therefore, it is likely that the "specific binding" of CNTs with high functionalization density governs the catalytic activity of α-ChT. It is also imperative to determine the functionalization density carefully before conducting any nanotoxicity evaluation studies because this attribute of CNTs regulates the enzymatic activity and may eventually decide the in vivo toxicity. Besides, it is meaningless to talk about how a certain property functions without strictly controlling other variable properties of nanomaterials. It may be easier for the researchers to approach the reliable nanotoxicological results if we keep in mind the principle of a single variable.

CONCLUSIONS

Carboxylized CNTs were found to bind with α-ChT, and the binding characteristics varied with the surface functionalization density of CNTs. The intrinsic fluorescence of the protein was quenched in a static way, and the main interaction between α-ChT and CNTs was an electrostatic association mixing with $\pi-\pi$ stacking. Minor secondary structural changes were observed with the reduction of the α-helix and the increment of the β-sheet, and the binding was mostly reversible. CNTs inhibited the enzymatic activity, and the surface carboxyl density played an important role in this process. Noncompetitive-like inhibition in enzymatic activities was induced by CNTs with low functionalization density, whereas competitive-like inhibition was caused by CNTs with high functionalization density. Therefore, the surface functionalization density of CNTs had significant influences on their biological effects.

ASSOCIATED CONTENT

Supporting Information

The Supporting Information is available free of charge on the ACS Publications website at DOI: 10.1021/acsami.5b05895.

High-resolution TEM images of CNT surfaces and the conjugates with protein, steady-state and time-resolved fluorescence spectra of α-ChT−CNTs interactions, and enzymatic activity of α-ChT at different NaCl concentrations (PDF)

AUTHOR INFORMATION

Corresponding Author

*E-mail: zhouqf@rcees.ac.cn. Fax/Tel: +86-10-62849334.

Notes

The authors declare no competing financial interest.

ACKNOWLEDGMENTS

We thank Dr. Gang Liang for technical assistance on AFM. This work was accomplished under financial support of the National Basic Research Program of China (Grant 2011CB936001), National Natural Science Foundation of China (Grants 21477153, 21137002, and 21307124), Major International (Regional) Joint Project (Grant 21461142001), and Strategic Priority Research Program of the Chinese Academy of Science (Grant 14040302).

REFERENCES

(1) Ursini, C. L.; Cavallo, D.; Fresegna, A. M.; Ciervo, A.; Maiello, R.; Buresti, G.; Casciardi, S.; Tombolini, F.; Bellucci, S.; Iavicoli, S. Comparative Cyto-Genotoxicity Assessment of Functionalized and Pristine Multiwalled Carbon Nanotubes on Human Lung Epithelial Cells. *Toxicol. In Vitro* **2012**, *26* (6), 831−840.

(2) Bussy, C.; Pinault, M.; Cambedouzou, J.; Landry, M. J.; Jegou, P.; Mayne-L'hermite, M.; Launois, P.; Boczkowski, J.; Lanone, S. Critical Role of Surface Chemical Modifications Induced by Length Shortening on Multi-Walled Carbon Nanotubes-Induced Toxicity. *Part. Fibre Toxicol.* **2012**, *9*, 46.

(3) Wang, G.; Zhang, J. P.; Dewilde, A. H.; Pal, A. K.; Bello, D.; Therrien, J. M.; Braunhut, S. J.; Marx, K. A. Understanding and Correcting for Carbon Nanotube Interferences with a Commercial LDH Cytotoxicity Assay. *Toxicology* **2012**, *299* (2−3), 99−111.

(4) Boczkowski, J.; Lanone, S. Respiratory Toxicities of Nanomaterials - A Focus on Carbon Nanotubes. *Adv. Drug Delivery Rev.* **2012**, *64* (15), 1694−1699.

(5) Wang, X.; Xia, T. A.; Ntim, S. A.; Ji, Z. X.; George, S.; Meng, H. A.; Zhang, H. Y.; Castranova, V.; Mitra, S.; Nel, A. E. Quantitative Techniques for Assessing and Controlling the Dispersion and Biological Effects of Multiwalled Carbon Nanotubes in Mammalian Tissue Culture Cells. *ACS Nano* **2010**, *4* (12), 7241−7252.

(6) Møller, P.; Christophersen, D. V.; Jensen, D. M.; Kermanizadeh, A.; Roursgaard, M.; Jacobsen, N. R.; Hemmingsen, J. G.; Danielsen, P. H.; Cao, Y.; Jantzen, K.; Klingberg, H.; Hersoug, L.-G.; Loft, S. Role of Oxidative Stress in Carbon Nanotube-Generated Health Effects. *Arch. Toxicol.* **2014**, *88* (11), 1939−1964.

DOI: 10.1021/acsami.5b05895
ACS Appl. Mater. Interfaces 2015, 7, 18880−18890

(7) Xu, J. G.; Alexander, D. B.; Futakuchi, M.; Numano, T.; Fukamachi, K.; Suzui, M.; Omori, T.; Kanno, J.; Hirose, A.; Tsuda, H. Size- and Shape-Dependent Pleural Translocation, Deposition, Fibrogenesis, and Mesothelial Proliferation by Multiwalled Carbon Nanotubes. *Cancer Sci.* **2014**, *105* (7), 763−769.
(8) Zhao, X.; Liu, R. Recent Progress and Perspectives on the Toxicity of Carbon Nanotubes at Organism, Organ, Cell, and Biomacromolecule Levels. *Environ. Int.* **2012**, *40*, 244−255.
(9) Song, M. Y.; Wang, F. B.; Zeng, L. Z.; Yin, J. F.; Wang, H. L.; Jiang, G. B. Co-exposure of Carboxyl-Functionalized Single-Walled Carbon Nanotubes and 17 alpha-Ethinylestradiol in Cultured Cells: Effects on Bioactivity and Cytotoxicity. *Environ. Sci. Technol.* **2014**, *48* (23), 13978−13984.
(10) Antonelli, A.; Serafini, S.; Menotta, M.; Sfara, C.; Pierige, F.; Giorgi, L.; Ambrosi, G.; Rossi, L.; Magnani, M. Improved Cellular Uptake of Functionalized Single-Walled Carbon Nanotubes. *Nanotechnology* **2010**, *21* (42), 425101.
(11) Luan, B.; Zhou, R. Nanopore-Based Sensors for Detecting Toxicity of a Carbon Nanotube to Proteins. *J. Phys. Chem. Lett.* **2012**, *3* (17), 2337−2341.
(12) Ali-Boucetta, H.; Kostarelos, K. Carbon Nanotubes in Medicine & Biology - Therapy and Diagnostics Preface. *Adv. Drug Delivery Rev.* **2013**, *65* (15), 1897−1898.
(13) Ali-Boucetta, H.; Kostarelos, K. Pharmacology of Carbon Nanotubes: Toxicokinetics, Excretion and Tissue Accumulation. *Adv. Drug Delivery Rev.* **2013**, *65* (15), 2111−2119.
(14) Sacchetti, C.; Motamedchaboki, K.; Magrini, A.; Palmieri, G.; Mattei, M.; Bernardini, S.; Rosato, N.; Bottini, N.; Bottini, M. Surface Polyethylene Glycol Conformation Influences the Protein Corona of Polyethylene Glycol-Modified Single-Walled Carbon Nanotubes: Potential Implications on Biological Performance. *ACS Nano* **2013**, *7* (3), 1974−1989.
(15) Skakalova, V.; Dettlaff-Weglikowska, U.; Roth, S. Gamma-Irradiated and Functionalized Single Wall Nanotubes. *Diamond Relat. Mater.* **2004**, *13* (2), 296−298.
(16) Zhao, X. C.; Liu, R. T.; Chi, Z. X.; Teng, Y.; Qin, P. F. New Insights into the Behavior of Bovine Serum Albumin Adsorbed onto Carbon Nanotubes: Comprehensive Spectroscopic Studies. *J. Phys. Chem. B* **2010**, *114* (16), 5625−5631.
(17) Ohshima, H. Henry's Function for Electrophoresis of a Cylindrical Colloidal Particle. *J. Colloid Interface Sci.* **1996**, *180* (1), 299−301.
(18) Gu, Q.; Kenny, J. E. Improvement of Inner Filter Effect Correction Based on Determination of Effective Geometric Parameters Using a Conventional Fluorimeter. *Anal. Chem.* **2009**, *81* (1), 420−426.
(19) Cheng, X. X.; Lui, Y.; Zhou, B.; Xiao, X. H.; Liu, Y. Probing the Binding Sites and the Effect of Berbamine on the Structure of Bovine Serum Albumin. *Spectrochim. Acta, Part A* **2009**, *72* (5), 922−928.
(20) Hu, Y. J.; Liu, Y.; Xiao, X. H. Investigation of the Interaction between Berberine and Human Serum Albumin. *Biomacromolecules* **2009**, *10* (3), 517−521.
(21) Greenfield, N. J. Using Circular Dichroism Spectra to Estimate Protein Secondary Structure. *Nat. Protoc.* **2007**, *1* (6), 2876−2890.
(22) Rubinow, S. I.; Lebowitz, J. L. Time-Dependent Michaelis-Menten Kinetics for an Enzyme-Substrate-Inhibitor System. *J. Am. Chem. Soc.* **1970**, *92* (13), 3888−3893.
(23) Cornish-Bowden, A.; Eisenthal, R. Statistical Considerations in Estimation of Enzyme Kinetic-Parameters by Direct Linear Plot and Other Methods. *Biochem. J.* **1974**, *139* (3), 721−730.
(24) Guo, J. X.; Li, Y. G.; Wu, S. W.; Li, W. X. The Effects of Gamma-Irradiation Dose on Chemical Modification of Multi-Walled Carbon Nanotubes. *Nanotechnology* **2005**, *16* (10), 2385−2388.
(25) Karajanagi, S. S.; Vertegel, A. A.; Kane, R. S.; Dordick, J. S. Structure and Function of Enzymes Adsorbed onto Single-Walled Carbon Nanotubes. *Langmuir* **2004**, *20* (26), 11594−11599.
(26) Ge, C.; Du, J.; Zhao, L.; Wang, L.; Liu, Y.; Li, D.; Yang, Y.; Zhou, R.; Zhao, Y.; Chai, Z.; Chen, C. Binding of Blood Proteins to Carbon Nanotubes Reduces Cytotoxicity. *Proc. Natl. Acad. Sci. U. S. A.* **2011**, *108* (41), 16968−16973.
(27) Yonamine, Y.; Yoshimatsu, K.; Lee, S.-H.; Hoshino, Y.; Okahata, Y.; Shea, K. J. Polymer Nanoparticle-Protein Interface. Evaluation of the Contribution of Positively Charged Functional Groups to Protein Affinity. *ACS Appl. Mater. Interfaces* **2013**, *5* (2), 374−379.
(28) Ball, E. G. The Composition of Pancreatic Juice and Blood Serum as Influenced by the Injection of Acid and Base. *J. Biol. Chem.* **1930**, *86* (2), 0433−0448.
(29) Sun, X.; Feng, Z.; Hou, T.; Li, Y. Mechanism of Graphene Oxide as an Enzyme Inhibitor from Molecular Dynamics Simulations. *ACS Appl. Mater. Interfaces* **2014**, *6* (10), 7153−7163.
(30) Subramanyam, R.; Gollapudi, A.; Bonigala, P.; Chinnaboina, M.; Amooru, D. G. Betulinic Acid Binding to Human Serum Albumin: A Study of Protein Conformation and Binding Affinity. *J. Photochem. Photobiol., B* **2009**, *94* (1), 8−12.
(31) Zhao, X.; Lu, D.; Hao, F.; Liu, R. Exploring the Diameter and Surface Dependent Conformational Changes in Carbon Nanotube-Protein Corona and the Related Cytotoxicity. *J. Hazard. Mater.* **2015**, *292* (0), 98−107.
(32) Li, S.; Aphale, A. N.; Macwan, I. G.; Patra, P. K.; Gonzalez, W. G.; Miksovska, J.; Leblanc, R. M. Graphene Oxide as a Quencher for Fluorescent Assay of Amino Acids, Peptides, and Proteins. *ACS Appl. Mater. Interfaces* **2012**, *4* (12), 7069−7075.
(33) Bourassa, P.; Kanakis, C. D.; Tarantilis, P.; Pollissiou, M. G.; Tajmir-Riahi, H. A. Resveratrol, Genistein, and Curcumin Bind Bovine Serum Albumin. *J. Phys. Chem. B* **2010**, *114* (9), 3348−3354.
(34) Liu, Y.; Ji, F.; Liu, R. The Interaction of Bovine Serum Albumin with Doxorubicin-Loaded Superparamagnetic Iron Oxide Nanoparticles: Spectroscope and Molecular Modelling Identification. *Nanotoxicology* **2013**, *7* (1), 97−104.
(35) Nepal, D.; Geckeler, K. E. Proteins and Carbon Nanotubes: Close Encounter in Water. *Small* **2007**, *3* (7), 1259−1265.
(36) Mu, Q. X.; Liu, W.; Xing, Y. H.; Zhou, H. Y.; Li, Z. W.; Zhang, Y.; Ji, L. H.; Wang, F.; Si, Z. K.; Zhang, B.; Yan, B. Protein Binding by Functionalized Multiwalled Carbon Nanotubes is Governed by the Surface Chemistry of Both Parties and the Nanotube Diameter. *J. Phys. Chem. C* **2008**, *112* (9), 3300−3307.
(37) Zhong, J.; Song, L.; Meng, J.; Gao, B.; Chu, W. S.; Xu, H. Y.; Luo, Y.; Guo, J. H.; Marcelli, A.; Xie, S. S.; Wu, Z. Y. Bio-Nano Interaction of Proteins Adsorbed on Single-Walled Carbon Nanotubes. *Carbon* **2009**, *47* (4), 967−973.
(38) Charbonneau, D.; Beauregard, M.; Tajmir-Riahi, H. A. Structural Analysis of Human Serum Albumin Complexes with Cationic Lipids. *J. Phys. Chem. B* **2009**, *113* (6), 1777−1784.
(39) Zhao, X.; Liu, R.; Teng, Y.; Liu, X. The Interaction between Ag+ and Bovine Serum Albumin: A Spectroscopic Investigation. *Sci. Total Environ.* **2011**, *409* (5), 892−897.
(40) Zhao, X.; Sheng, F.; Zheng, J.; Liu, R. Composition and Stability of Anthocyanins from Purple Solanum tuberosum and Their Protective Influence on Cr(VI) Targeted to Bovine Serum Albumin. *J. Agric. Food Chem.* **2011**, *59* (14), 7902−7909.
(41) De Diego, T.; Lozano, P.; Gmouh, S.; Vaultier, M.; Iborra, J. L. Fluorescence and CD Spectroscopic Analysis of the alpha-Chymotrypsin Stabilization by the Ionic Liquid, 1-Ethyl-3-Methylimidazolium Bis [(Trifluoromethyl) Sulfonyl] Amide. *Biotechnol. Bioeng.* **2004**, *88* (7), 916−924.
(42) Sandanaraj, B. S.; Vutukuri, D. R.; Simard, J. M.; Klaikherd, A.; Hong, R.; Rotello, V. M.; Thayumanavan, S. Noncovalent Modification of Chymotrypsin Surface Using an Amphiphilic Polymer Scaffold: Implications in Modulating Protein Function. *J. Am. Chem. Soc.* **2005**, *127* (30), 10693−10698.
(43) De, M.; Chou, S. S.; Dravid, V. P. Graphene Oxide as an Enzyme Inhibitor: Modulation of Activity of α-Chymotrypsin. *J. Am. Chem. Soc.* **2011**, *133* (44), 17524−17527.
(44) Roy, R.; Sandanaraj, B. S.; Klaikherd, A.; Thayumanavan, S. Tuning Substrate Selectivity of a Cationic Enzyme Using Cationic Polymers. *Langmuir* **2006**, *22* (18), 7695−7700.

DOI: 10.1021/acsami.5b05895
ACS Appl. Mater. Interfaces 2015, 7, 18880−18890

(45) Zhang, B.; Xing, Y.; Li, Z.; Zhou, H.; Mu, Q.; Yan, B. Functionalized Carbon Nanotubes Specifically Bind to alpha-Chymotrypsin's Catalytic Site and Regulate Its Enzymatic Function. *Nano Lett.* **2009**, *9* (6), 2280−2284.

DOI: 10.1021/acsami.5b05895
ACS Appl. Mater. Interfaces 2015, 7, 18880−18890